Pergamon

Cement and Concrete Research 31 (2001) 1437–1447

CEMENT AND CONCRETE RESEARCH

Adiabatically cured, alkali-activated cement-based wasteforms containing high levels of fly ash
Formation of zeolites and Al-substituted C-S-H

A.R. Brough[a,*], A. Katz[a,1], G.-K. Sun[a], L.J. Struble[a,b], R.J. Kirkpatrick[a,c], J.F. Young[a,b]

[a]*Center for Advanced Cement-Based Materials, University of Illinois at Urbana-Champaign, 204 Ceramics Building, 105 South Goodwin Avenue, Urbana, IL 61801, USA*

[b]*Department of Civil Engineering, University of Illinois at Urbana-Champaign, Urbana, IL 61801, USA*

[c]*Department of Geology, University of Illinois at Urbana-Champaign, Urbana, IL 61801, USA*

Received 7 July 2000; accepted 20 June 2001

Abstract

Cementitious binder compositions with high fly ash contents proposed for immobilization of highly alkaline low-level radioactive waste solutions have significantly different chemistry and behavior than normal Portland cement pastes. In this paper, we investigate the mineralogy of a simulated wasteform proposed for the immobilization of the tank wastes stored at the Hanford Reservation, Washington State, USA. These solutions have very high (multimolar) concentrations of sodium, aluminate, phosphate, carbonate, nitrate, and nitrite ions. The cementitious blend proposed to solidify this solution contains a high proportion of fly ash to avoid the large heat output that would be associated with the hydration of a neat Portland cement. In addition to calcium silicate hydrate (C-S-H), the binding phase normally formed by hydrating cements, zeolites also formed during adiabatic curing up to 90°C. The zeolites, sodalite and Na-P1 (gismondine framework), immobilize part of the sodium in the system. Compared to C-S-H in ordinary Portland cement (OPC), the C-S-H in this system, which had a layer spacing of 1.1 nm, was more crystalline, and had a longer chain length and a higher aluminum content. Changing the curing conditions had a large effect on early age mineralogy, for example, traces of chabazite are formed on isothermal curing at 90°C. The long-term mineralogy depended mainly on the final curing temperature.

Keywords: Alkali-activated cement; Fly ash; Radioactive waste; Calcium silicate hydrate; C-S-H; Zeolite

1. Introduction

Cementitious materials are the basis of potential solid wasteforms for many nuclear and toxic wastes. Blends of Portland cement with mineral admixtures slow the rate of transport of water and dissolved species through the solid matrix. In addition, the hydration products, principally portlandite (calcium hydroxide) and calcium silicate hydrate (C-S-H),[2] buffer the pore solution to high pH, and under these conditions many toxic species such as heavy metals are precipitated as hydroxides [1]. A previous note [2] described the mineralogy of a cement-based wasteform in which zeolites and feldspathoid minerals form in abundance along with an aluminous C-S-H. The wasteform was developed for immobilization of low-level radioactive waste solutions currently stored at the Hanford Reservation in Washington State, USA. This cement blend is high in fly ash and here is hydrated with a highly alkaline simulated waste solution, and cured at temperatures up to 90°C [3]. This system is likely to be representative of many systems in which the solution is chemically complex and highly alkaline and in which heat evolution is a significant concern. The formulation has been shown to provide effective immobilization of a range of hazardous species. However, due to the unusual and complicated chemical compositions of these wastes, the widely varying cement blends, and the

* Corresponding author. Departments of Civil Engineering and Materials, University of Leeds, Leeds LS2 9JT, UK. Tel.: +44-113-233-2306; fax: +44-113-233-2265.

E-mail address: a.r.brough@leeds.ac.uk (A.R. Brough).

[1] Present address: Department of Civil Engineering, Technion-Israel Institute of Technology, Haifa 32000, Israel.

[2] Ceramic notation: C = CaO, S = SiO_2, H = H_2O, A = Al_2O_3, F = Fe_2O_3.

0008-8846/01/$ – see front matter
PII: S0008-8846(01)00589-0

potentially high temperature curing conditions, relatively little is known about the chemical and mineralogical composition of the solid phases and the long-term behavior of these wasteforms.

The formation of zeolites and related phases in cement systems is of considerable interest because significant quantities of water can be immobilized in the zeolite pores, and the zeolites can absorb significant amounts of cations [4]. Such in situ zeolite formation has been observed previously in alkali-activated blended cement systems with high levels of pozzolonic admixtures [5–7]. Hoyle and Grutzeck [7] have demonstrated the potential for removal of cesium from solution by use of alkali-activated calcium aluminosilicate glasses. Alkali activation of mixed calcium aluminate/silica fume cements has been used to immobilize cesium ions from solution [8,9].

In this paper, the mineralogy of a simulated Hanford wasteform is considered in detail. The zeolites that form are identified, their relationship to AFm formation and disappearance is described, and the differences between the C-S-H formed in this system and that formed by the hydration of ordinary Portland cement (OPC) at ambient temperatures are considered. The wasteform begins to lose strength after about 14 days hydration, and thus the time evolution of the mineralogy and the effects of various curing regimens are studied. Other papers have described aspects of the chemistry and microstructure of similar simulated wasteforms [10–15].

2. Materials and methods

2.1. Solution

The solution utilized in this study (Table 1) was designed to simulate the composition of one particular tank of low-level waste solution currently stored at Hanford [3,16,17]; it is highly alkaline and has a very high concentration of dissolved salts. There is a high level of short-lived isotopes in the tank, giving rise to some radiolytic heating; however the activity due to long-lived isotopes is low, leading to the tank being classified as low-level waste. For the simulated solution, the components were added sequentially at 45°C, each being allowed to dissolve fully before the next was added. The final solution was stored at 45°C to prevent the precipitation of sodium phosphate, which occurred if the solution was allowed to cool. Solutions were not kept longer than 1 week, since gibbsite sometimes precipitated at later ages. Other papers [2,11] describe the use of a simplified solution containing only those species indicated in bold type in Table 1. Table 2 shows the molarity of the major species in the solution.

Table 1
Composition of the full simulated low-level waste solution

Compound	g/l
NaOH	**74.80**
$Al(NO_3)_3 \cdot 9H_2O$	**128.00**
$Na_3PO_4 \cdot 12H_2O$	**74.40**
$NaNO_2$	**36.90**
Na_2CO_3	**36.20**
$NaNO_3$	8.58
KCl	1.83
NaCl	2.50
$Na_3Citrate \cdot 2H_2O$	2.50
$Na_2B_4O_7$	0.13
Na_2SO_4	3.89
$Ni(NO_3)_2 \cdot 6H_2O$	0.30
$Ca(NO_3)_2 \cdot 4H_2O$	0.44
$Na_4(EDTA) \cdot 2H_2O$	1.42
$Na_3(HEDTA)$	5.29
Glycolic acid	0.65
$Mg(NO_3)_2 \cdot 6H_2O$	0.03

Components used to make up a simplified solution are shown in bold type.

Table 2
Concentration of the most important species in the simulated tank waste solution

Major species	Molarity
Na^+	4
Nitrate	1.2
Nitrite	0.5
Carbonate	0.35
Aluminate	0.35
Phosphate	0.20
pH	>13

2.2. Cementitious binder

The wasteform samples were generated by the reaction of the simulated waste solution at elevated temperature with a preblended mixture of cement, fly ash, and clay, with the proportions given in Table 3. This dry blend was developed [16,17] to provide a wasteform meeting engineering and environmental specifications for immobilization of the highly alkaline low-level radioactive tank wastes currently stored at Hanford. The low cement content (20.7%) and high fly ash content (68.3%) is required to limit to acceptable values the nearly adiabatic heat rise occurring during reaction in large monoliths. The clay thickens the mixture and stops segregation prior to set. The formulation meets a minimum 28-day strength of 3.5 MPa and a maximum temperature under adiabatic curing of 90°C. The solids

Table 3
Composition of the dry blend

Material	Amount (%)	Density	Description	Supplier
Cement	20.7	3.21	ASTM Type II	Ash Grove Cement (Durkee, OR)
Fly ash	68.3	2.38	Centralia Class F	Ross Sand and Gravel (Portland, OR)
Clay	11.0	2.24	Attapulgite Clay	Engelhard (Inselin, NJ)

Table 4
Oxide analyses by XRF spectroscopy of the raw materials

Oxide	Cement	Fly ash	Clay
SiO_2	22.17	46.13	59.71
Al_2O_3	3.24	25.02	9.05
Fe_2O_3	4.24	7.25	3.17
CaO	64.48	8.02	3.13
MgO	1.13	1.81	11.21
K_2O	0.52	0.63	0.83
Na_2O	0.15	4.74	0.07
TiO_2	0.23	4.70	0.42
P_2O_5	0.12	0.42	1.47
MnO	0.06	0.03	0.05
SO_3	2.14	0.12	<0.1
LOI	1.20	0.53	10.64

were preblended by hand-mixing; the dry blend was then placed in a cylindrical container and rotated end-over-end at room temperature overnight for complete mixing.

Elemental compositions of the individual components (Table 4) were determined by X-ray fluorescence (XRF) spectroscopy after fusion with lithium borate, and with use of appropriate NIST-traceable standards for calibration. The fly ash contains a relatively high level of Ca compared to many USA Class F fly ashes. The particle size distributions of the cement and fly ash were measured by sieve analysis (Table 5) and by sedimentation (Fig. 1). The median equivalent spherical particle diameters were 7 and 13 μm for the cement and fly ash, respectively. The clay is significantly finer but its particle size distribution was not determined.

2.3. Wasteform mixing

A high solution/solid ratio of 1.0 ml/g was used to maximize the loading of the waste solution, and minimize the volume increase after treatment. The actual water/binder ratio was slightly lower due to the high salt content of the solution. Mixing took place at 45°C, a typical upper temperature limit during mixing of the solids and radiolytically heated liquid in practice [3]. The solids, solution, and mixing implements were all equilibrated to 45°C in a temperature-controlled room prior to mixing to facilitate

Table 5
Sieve analysis of the cement and fly ash

	Percent of material in range	
Size/μm	Cement	Fly ash
>50	0	10
30–50	2	16
20–30	6	12
10–20	24	22
5–10	30	22
2–5	22	N/A
1–2	10	N/A
<1	6	N/A
<5	N/A	18

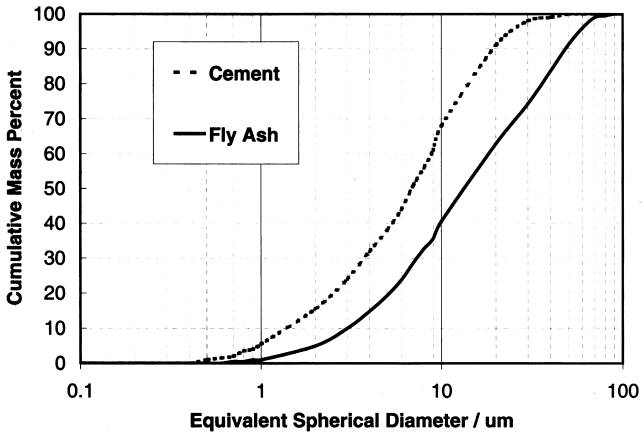

Fig. 1. Particle size distributions by sedimentation of the cement and fly ash.

isothermal and adiabatic calorimetry. The liquid was poured into the mixing bowl of a planetary mixer (Hobart Model N-50) and the solid added gradually over 15 s, with slow-speed stirring. The paddle and bowl were then scraped down, and mixing continued for 2–3 min at intermediate speed, or until the solids appeared to be fully dispersed.

The wasteform samples were cast into 25-mm diameter plastic tubes, which were sealed and placed into a custom-built programmable oven equipped with a ramp and hold controller. Unless otherwise noted, the temperature was raised to 90°C in a series of ramps (line (b) in Fig. 2) over 3 days to simulate the expected adiabatic temperature profile [16,17]. After 3 days, the exothermic hydration was largely complete, and the sample tubes were transferred to an isothermal oven at 90°C for long-term curing. The sealed sample tubes were stored in sealed containers partly filled with water at a relative humidity of >95% to ensure that loss of water vapor would not occur. At each testing age, 50-mm long sections were sawn from at least three cylinders for

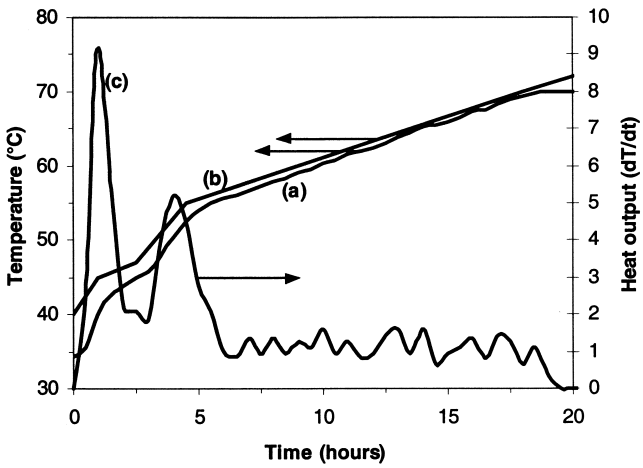

Fig. 2. Semiadiabatic calorimetry, corrected for heat loss to the dewar (after Ref. [3]) showing (a) sample temperature, (b) programmed oven temperature used for "adiabatic curing" of samples, and (c) rate of increase of sample temperature, calculated from curve (a).

compressive strength measurements. Samples were also studied by powder X-ray diffraction (XRD) and by solid-state magic angle spinning nuclear magnetic resonance (MAS NMR) spectroscopy. Samples for isothermal calorimetry at 45°C were taken directly after mixing.

2.4. Characterization techniques

Samples for NMR were beneficiated by magnetic separation of ferromagnetic and strongly paramagnetic particles to reduce linebroadening. ^{29}Si, ^{27}Al, ^{31}P, and ^{23}Na MAS NMR spectra were acquired without decoupling using home-built spectrometers equipped with Oxford Instruments narrow bore superconducting magnets and Nicolet 1280 computers. ^{29}Si spectra were acquired at 99 MHz (7.4 T) using a standard or fast spinning Doty MAS probe. The samples were packed in 5- or 7-mm diameter zirconia rotors and MAS was performed at 4–6 kHz. A radio frequency (RF) field of approximately 40 kHz was used, and all spectra were acquired with 45° pulses. ^{29}Si chemical shifts are reported to the nearest 0.5 ppm, and are referenced to TMS. ^{31}P, ^{27}Al, and ^{23}Na spectra were acquired at 116 MHz (7.4 T), 130 MHz (11.7 T), and 132 MHz (11.7 T), respectively, using a Doty fast spinning MAS probe. The samples were packed in 5-mm diameter silicon nitride or alumina rotors and MAS was performed at approximately 10 kHz. An RF field of approximately 60 kHz was used; spectra for ^{31}P were acquired with 45° pulses, while for the quadrupolar species, ^{27}Al and ^{23}Na, all spectra were acquired with short (1 μs) pulses in order to minimize intensity distortions arising from quadrupolar effects [18]. ^{31}P, ^{27}Al, and ^{23}Na chemical shifts are reported to the nearest 1 ppm, and referenced to phosphoric acid, 1 M $Al(H_2O)_6^{3+}$ solution and solid NaCl, respectively.

XRD patterns were obtained using a Rigaku powder diffractometer (Model D-max II) with monochromated Cu($K_{\alpha 1}$) radiation. Samples were finely powdered and surface-dried in air, unless otherwise indicated. Peaks were assigned by reference to the JCPDS database. Isothermal calorimetry was performed at 45°C using an isothermal conduction calorimeter (Quadrel K200, Digital Site Systems, Pittsburgh, PA). Samples were transferred to the calorimeter directly after mixing, but ~30 min were required before the calorimeter reached thermal equilibrium. Compressive strength measurements were determined using a multipurpose testing machine (Instron).

3. Results and discussion

3.1. Characterization of binder components

The Bogue composition of the Portland cement calculated using the procedure described in ASTM C-150 is 61.0% C_3S, 18.5% C_2S, 1.5% C_3A, and 13.0% C_4AF. The XRD pattern (Fig. 3(a)) shows the usual phases. Some of the gypsum has been dehydrated, and a small amount of portlandite is also present. The ^{29}Si MAS NMR spectra of the cement has a composite peak centered at ~ − 72 ppm due to the Q^0 species[3] in the alite and belite. The cement exhibited only a very weak ^{27}Al MAS NMR signal, with broad peaks at approximately 90 and 12 ppm. The loss on ignition (LOI) of 1.2% indicates that storage conditions for the cement have been satisfactory and that no substantial hydration or carbonation has occurred.

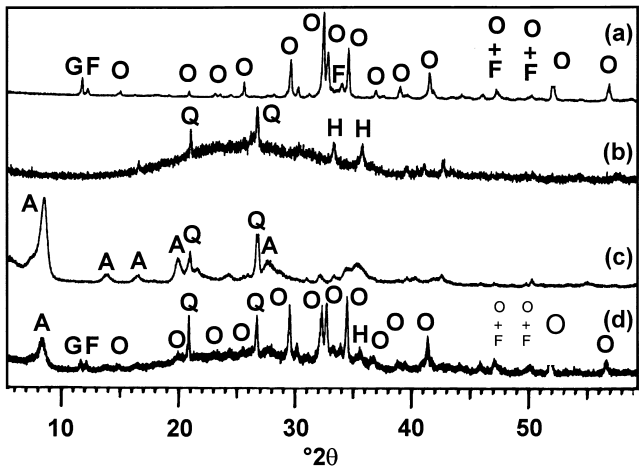

Fig. 3. XRD spectra (Cu($K_{\alpha 1}$)) of the dry raw materials showing: (a) cement, (b) fly ash, (c) attapulgite clay, and (d) the dry blended solids. A = attapulgite; O = alite and belite; Q = quartz; G = gypsum; F = ferrite; H = hematite.

The major feature of the XRD pattern of the Class F fly ash (Fig. 3(b)) was the broad diffuse peak centered at about 26° 2θ due to the glassy phase of the fly ash. The position of this peak is consistent with a glassy phase having a relatively low calcium content [19]. The small sharp peaks are due to traces of crystalline materials, predominantly quartz, mullite, hematite, and magnetite. A scanning electron microscopy (SEM) examination showed occasional large crystals of quartz in the fly ash. The ^{29}Si MAS NMR spectrum gives a very broad peak centered at ~ − 97 ppm due to partially depolymerized silica or aluminosilicate species in the glassy phase. The ^{27}Al MAS NMR of the fly ash contained a single broad resonance at approximately 60 ppm assigned to tetrahedral (four coordinated, Al[4]) species contained in the fly ash glass. The ^{23}Na MAS NMR spectrum of the unreacted fly ash contained a single broad peak at ~ − 25 ppm with a half-height linewidth of approximately 2.5 kHz. There was very little ^{23}Na signal for the cement or clay.

The XRD pattern of the attapulgite clay (Fig. 3(c)) showed a broad peak due to the clay (similar to those for palygorskite) and a few weak peaks due to traces of quartz. The ^{29}Si MAS NMR spectrum contained two peaks with chemical shifts of approximately − 91.2 and − 97.2 ppm,

[3] In the Q^n notation used to describe silicate polymerization, Q signifies a silicate tetrahedron and n signifies the number of oxygen bridging to adjacent tetrahedra.

which can be assigned to the two differently coordinated silicate sites in the structure. The ^{27}Al MAS NMR spectrum showed a sharp peak at 7 ppm assigned to octahedral aluminum (six coordinated, Al[6]).

The XRD pattern of the dry blended solids (Fig. 3(d)) contained peaks due to the various crystalline phases in the individual solid materials discussed above and a broad diffuse reflection centered at about 26° 2θ due to the glassy phase of the fly ash.

3.2. Characterization of mature wasteforms

3.2.1. X-ray diffraction

The XRD pattern of the wasteform hydrated adiabatically for 12 months (Fig. 4(a)) showed major peaks due to sodalite and smaller peaks for Na-P1 zeolite. There were also well-resolved peaks due to C-S-H with a basal spacing of approximately 1.1 nm. This C-S-H is significantly more crystalline than the C-S-H formed during hydration of OPC at ambient temperature [20]. In addition, a broad peak centered at 31° 2θ may be due to poorly crystallized zeolitic material or residual fly ash glass. The identity of the relatively crystalline C-S-H has been confirmed by extraction using a solution containing 23 g salicylic acid in 100 ml methanol with 2.5 g of wasteform, which is known to dissolve C-S-H as well as anhydrous C_2S and C_3S [21,22]. The XRD pattern of the residual solid after extraction (Fig. 4(b)) shows peaks due primarily to the sodalite, zeolite, and calcite. The difference spectrum, which approximates the XRD pattern of the extracted material (Fig. 4(c)), is consistent with the data recorded in the JCPDS file (Card Number 19-1364) for 1.1 nm tobermorite, but only some of the peaks are observed, indicating significant structural disorder. Therefore, the material formed is best considered a relatively crystalline C-S-H with a layer spacing of 1.1 nm. This value contrasts with the typical C-S-H formed during hydration of OPC at ambient temperature, which has a layer spacing of 1.4 nm [20] and is significantly less crystalline. The extraction procedure has also attacked some of the other phases, causing partial loss of the Na-P1 zeolite. The broad peak centered at 31° 2θ is largely unaffected by the extraction procedure. In addition to the primary product phases, there were small and variable amounts of quartz, primarily from the fly ash, and calcite, probably arising from the carbonate in the waste solution and calcium released from the solid blend.

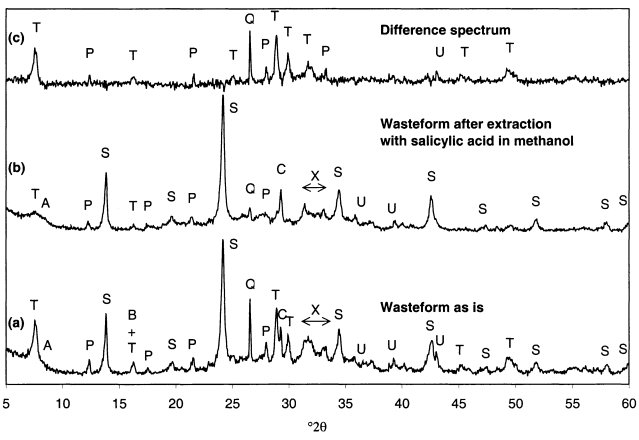

Fig. 4. XRD spectra (Cu($K_{\alpha 1}$)) showing: (a) the wasteform, hydrated adiabatically for the first 3 days and thereafter at 90°C for 1 year, (b) sample of (a) after extraction of C-S-H using a solution of salicylic acid in methanol, and (c) difference spectrum, giving an approximate XRD pattern for the extracted material. A = attapulgite; B = unreacted binder; C = calcite; P = Na-P1 zeolite; Q = quartz; S = sodalite; T = relatively crystalline C-S-H having a layer spacing of 1.1 nm; U = unassigned; X = various overlapping peaks, in region indicated by horizontal line.

3.2.2. Zeolite and feldspathoid phases

The zeolite Na-P1 is one of a series of synthetic P zeolites that are structurally related to natural zeolites, such as phillipsite and gismondine, all of which have close structural similarities. Na-P1 has the normal formula $Na_6Al_6Si_{10}O_{32}{\cdot}15H_2O$ with a gismondine structure. This structure is based on a "double-crankshaft" chain of linked tetrahedra in which the smallest structural unit is the four-ring $(Al,Si)_4O_8$ unit. These chains run parallel to both the *a*- and *b*-axes to form a framework with eight-ring apertures accessing intersecting channels [23]. It is readily synthesized in the $Na_2O-Al_2O_3-SiO_2-H_2O$ system at 60–150°C (e.g., from kaolinite and NaOH) and is also one product in the reaction of Class F fly ash, or fly ash–cement mixtures with 2.8 or 5 M NaOH at about 90°C [6], which is similar to the conditions used in this paper.

Sodalite is a feldspathoid mineral with a framework aluminosilicate structure based on cages containing an ordered arrangement of 24 Al,Si tetrahedra in equal abundance. It contains no essential water but does require both cations and anions to be present in the cages. Its nominal formula is $Na_6Si_6Al_6O_{24}{\cdot}2NaX{\cdot}nH_2O$ with the sodium salt encapsulated in the cages. The anion X can vary widely [24] and though Na(OH) (giving hydroxysodalite) is likely to predominate under the conditions of the wasteform, some $NaNO_3$, $NaNO_2$, and Na_2CO_3 might also be encapsulated. In addition, there may be some replacement of Na by Ca. The composition of the sodalite in our samples cannot be determined from the XRD patterns, because the peaks are relatively broad and overlap significantly, even after extraction of the C-S-H. Sodalite is not a zeolite, because the cages are densely packed (many zeolites have structures based on open packings of sodalite cages). Because of its relatively dense structure, the cations and anions in the cages are not readily exchanged, making it a relatively attractive phase for encapsulation of waste. In the absence of cement, cancrinite, a framework aluminosilicate related to sodalite by different stacking of layers, has been observed [25] under similar conditions. The close structural similarity between sodalite and cancrinite is well recognized and the two can coexist under certain synthetic conditions [24]. In this wasteform, however, sodalite is the predominant phase formed, as indicated by the presence

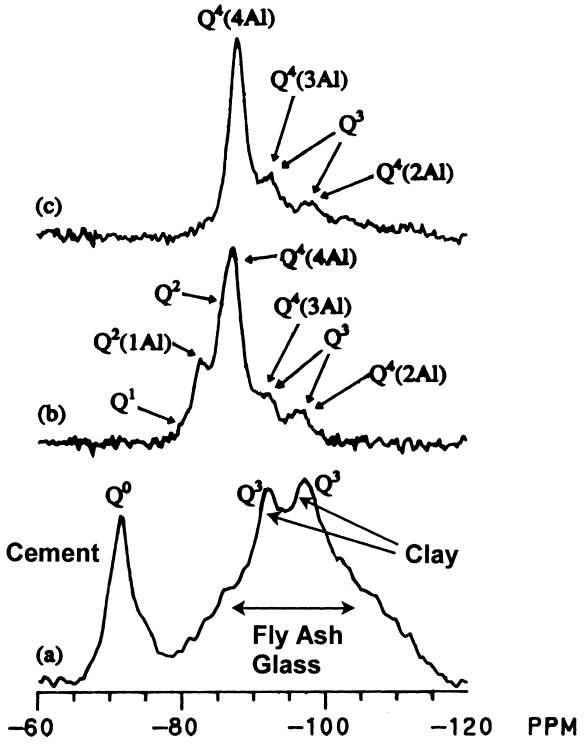

Fig. 5. ^{29}Si MAS NMR spectra acquired at 99 MHz showing (a) the dry blended solids, (b) the wasteform, hydrated adiabatically for the first 3 days and thereafter at 90°C for 1 year, and (c) as (b), but after extraction of C-S-H using a solution of salicylic acid in methanol.

of the (200) reflection at $\sim$19.5° 2θ, which is not found for cancrinites.

3.2.3. NMR spectroscopy

The ^{29}Si MAS NMR spectrum of the unreacted dry blended solids (Fig. 5(a)) contained peaks readily assignable to the individual components of the dry blend. The compound peak centered at -72 ppm arises from monomeric Q^0 silicate species in the anhydrous cement. The two peaks at -91.5 and -97.5 ppm arise from the two Q^3 species in the attapulgite clay, and the very broad peak centered at ~ -97 ppm arises from a continuous range of $Q^n(m\text{Al})$[4] species in the glassy phase of the fly ash. Integration of the areas of the different peaks indicates that there is significant loss of signal from the silicate species in the fly ash, probably due to the presence of paramagnetic species in its structure.

The ^{27}Al MAS NMR spectrum of the dry blended solids (Fig. 6(a)) consisted of two major peaks, a broad asymmetric Al[4] peak at $\sim$60 ppm and a sharper Al[6] peak at $\sim$7 ppm. By comparison with the individual components, the Al[4] is assigned to species in the glassy phase of the fly ash and the sharper Al[6] peak is assigned to species in the attapulgite clay.

The ^{29}Si MAS NMR spectra of the 1-year-old wasteform (Fig. 5(b)) contain resolved peaks at -82.5, -87, -92, and -97 ppm. In addition, there is a low peak at ~ -79 ppm, and the peak at ~ -87 ppm was skewed, with a shoulder to low field (~ -85 ppm). The resonances at ~ -79, ~ -82.5, and ~ -85 ppm can be assigned to Q^1, Q^2(1Al), and Q^2 species, respectively, in C-S-H chains with silica, partially substituted by aluminum. These assignments are made by comparison with spectra from samples of pure C-S-H [26,27] and from C-S-H containing a high level of aluminum substitution [28–30]. The ^{29}Si linewidths were large, indicating that the silicate species are very poorly crystalline. The spectrum after extraction of the C-S-H and calcium silicates using excess salicylic acid in methanol (Fig. 5(c)) contained a distinct peak at -87.5 ppm, which can be assigned to the Q^4(4Al) species of sodalite and possibly the Na-P1 zeolite. The peaks at ~ -92 and ~ -97.5 ppm include, respectively, contributions from Q^4(3Al) and Q^4(2Al) sites in the Na-P1 zeolite. There may be contributions from the two Q^3 species in attapulgite, but this phase has been largely removed during reaction.

The ^{27}Al MAS NMR spectrum of the aged wasteform (Fig. 6(b)) contained primarily a single resonance with maximum intensity at 62 ppm, corresponding to Al[4] species in the product phases. This peak had a much narrower linewidth than that of the Al[4] in the fly ash glass. It is not possible to resolve separate peaks for Al in the sodalite, zeolite, and C-S-H, due to peak overlap. The fraction of total Al substituted into the C-S-H, however, should be small relative to that in the zeolites, based on the ^{29}Si spectra. By comparison with Al[4] species in

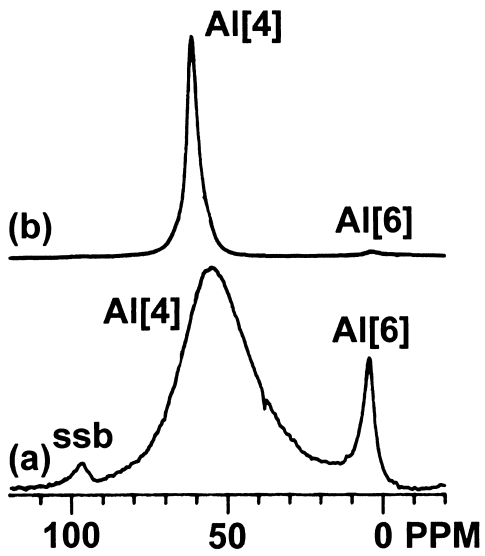

Fig. 6. ^{27}Al MAS NMR spectra acquired at 130 MHz showing (a) the dry blended solids and (b) the wasteform, hydrated adiabatically for the first 3 days and thereafter at 90°C for 1 year. ssb = spinning sideband.

[4] In the $Q^n(m\text{Al})$ notation used to describe aluminosilicate polymerization, Q signifies a silicate tetrahedron, n signifies the number of oxygen bridging to adjacent tetrahedra, and m denotes the number of adjacent tetrahedra that contain a central Al atom rather than Si.

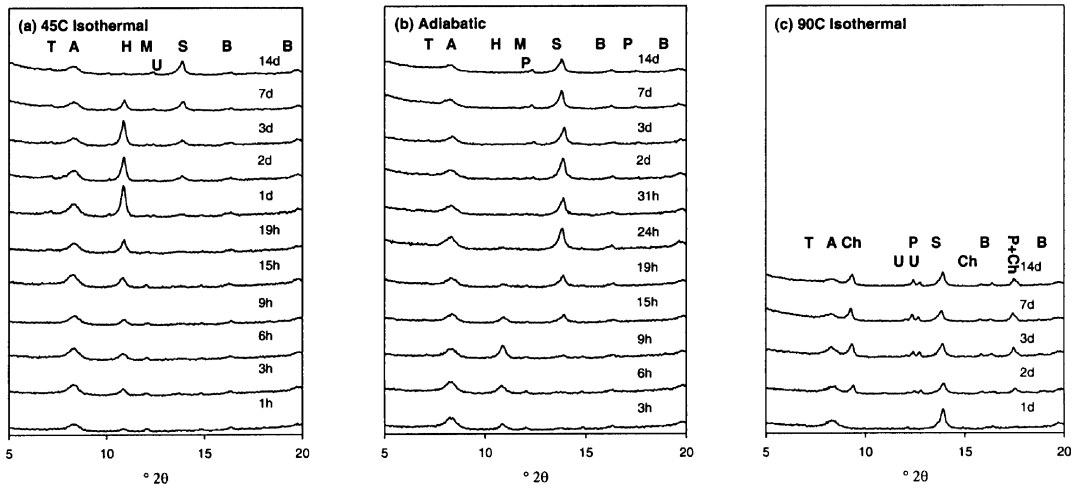

Fig. 7. XRD spectra ($Cu(K_{\alpha 1})$) of the wasteform hydrated: (a) isothermally at 45°C, (b) adiabatically for the first 3 days and thereafter at 90°C, and (c) isothermally at 90°C. Labels are as given for Fig. 4, additionally Ch = possibly chabazite; H and M = various AFm phases (probably H = hemicarboaluminate, M = full carbonate AFm).

other systems [28–30], we would expect the Al substituted into C-S-H to form a relatively broad peak between -55 and -75 ppm. In sodalite, the ^{29}Si and ^{27}Al shifts are correlated [31], and the observed ^{29}Si shift of -87.5 ppm predicts an ^{27}Al shift of approximately 62 ppm, which is indeed the observed Al[4] peak position. It appears, then, that the observed Al[4] peak at 62 ppm consists of a sharper peak due to Al[4] species in sodalite and a broader overlapping peak due to Al[4] sites substituted in C-S-H. The small peak at 7 ppm for the aged sample is probably due to a small amount of residual attapulgite, but could also indicate the presence of an AFm phase.

The ^{31}P MAS NMR spectra of a number of wasteform samples all contained a single peak at ~ 5 ppm, consistent with the presence of monophosphate groups in an inorganic solid. Thus, the phosphate originally present in solution, which would give a much sharper resonance, was precipitated. This observation is in agreement with earlier results [10,12] showing rapid loss of phosphate from solution in similar wastes. It is not possible to determine further details about the precipitated material, which was not observed by XRD.

The ^{23}Na MAS NMR spectra of the 1-year-old wasteform contain a single peak at ~ -10.5 ppm, with a half-height linewidth of about 1 kHz. (The raw materials gave only a broad weak signal at -25 ppm.) The chemical shift in the wasteform is consistent with ^{23}Na in solution [32], in sodalite cages [33], or in a mixture of products, as is expected from pore solution chemistry studies of similar systems [10,12]. In these studies, about half the sodium was immobilized into solid phases and the remainder was in the solution. A sample of sodalite imbibed with sodium nitrite synthesized in our laboratory gave a sharp peak at approximately -8.5 ppm. Note that ^{23}Na MAS NMR spectra can be difficult to interpret, because of quadrupolar effects and peak overlap, so assignments are tentative.

3.2.4. Gel composition

The microstructure of the gel formed in these pastes, as described previously [2], consisted of a relatively featureless space-filling gel in which relics of the fly ash grains were seen in fracture surfaces. The composition of the gel was highly variable [24,34]. Therefore, it was not possible to use analysis in the scanning electron microscope to determine compositions of individual phases. While XRD suggests the presence of particular phases, it should be noted that it is likely that there is substitution so that these phases do not have their ideal compositions.

The C-S-H in the 1-year-old wasteform contains few Q^1 species relative to the $Q^2(1Al)$ and Q^2 species (Fig. 7(b)), indicating that the aluminosilicate chains were quite long. The overlap of the peaks at -85 and -87.5 ppm makes quantification difficult, but an average aluminosilicate chain length of 10 or more can be estimated.[5] This is long compared with C-S-H formed by hydration of C_3S at 20°C, which has an average chain silicate length of approximately three at the same age [27].

Trimethylsilylation data did not indicate the presence of highly polymerized species [35]. This is to be expected, since aluminosilicate species are cleaved at the Al sites [36]. Thus, a chain with every third silicate site substituted with Al will analyze as dimer.

[5] We define the average chain length, L, from the ratio of middle-chain groups and end-chain groups, assuming no cross-linking Q^3 or Q^4 species. We include aluminate groups in this calculation, assuming that each aluminate group occupies a $Q^2(2Si)$ site, and that there are no chain-terminating aluminate groups. Then, $L = 2+(2I(Q^2)+3I(Q^2(1Al)))/I(Q^1)$.

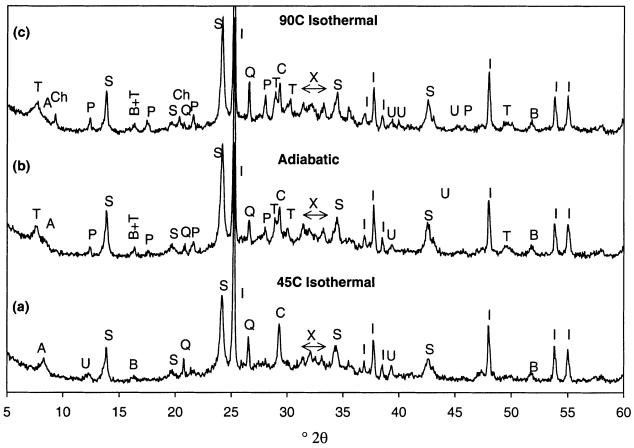

Fig. 8. XRD spectra ($Cu(K_{\alpha 1})$) for samples of the wasteform hydrated for 28 days (a) isothermally at 45°C, (b) adiabatically for the first 3 days and thereafter at 90°C, and (c) isothermally at 90°C. Labels are as given for Fig. 4, additionally I = TiO_2 (rutile) for intensity normalization.

3.3. Phase evolution

Analysis of wasteform samples withdrawn and quenched at early stages of hydration showed a complex evolution of the crystalline phases. Samples hydrated isothermally at 45°C (for comparison with the calorimetry data) and at 90°C, and heated from 45°C to 90°C over 3 days (simulated adiabatic hydration) were studied using powder XRD and MAS NMR spectroscopy. Selected regions of the XRD patterns showing representative peaks for the important species are presented in Fig. 7. The XRD patterns for the three curing conditions after 28-day reaction are shown in Fig. 8. Titanium dioxide was added as a quantitative standard, and all the samples were prepared in a similar manner and had a similar bulk chemical composition, allowing peak heights to be compared; full quantitative data were not available, however, since some of the phases present were only semicrystalline and for others, the exact composition was not known, so that quantitative standards could not be prepared. Hydration was stopped by grinding in methanol, and the samples were then air-dried and reground before mounting in the XRD sample holders.

The initial reaction product is an AFm phase, which gradually disappears with the concomitant formation of sodalite (Fig. 7). The maximum amount of AFm occurs at 1 day at 45°C and at 9 h under adiabatic conditions. However, the amount of sodalite continues to increase after AFm is no longer observed. AFt phases (ettringite), which form from tricalcium aluminate early in the hydration of conventional cement pastes, were not observed. AFm is a family of compounds based on a layer structure $[CaAl(OH)_6 \cdot H_2O]^+$ that is charge-balanced by anions located in the interlayer space. It forms in conventional cement pastes with SO_4^{2-} as the charge balancing anion, but here the *d*-spacing of 0.82 nm is consistent with hemicarboaluminate, which contains CO_3^{2-} and OH^- ions. Nevertheless, inclusion of NO_3^{3-}, NO_2^{2-}, or SO_4^{2-} cannot be ruled out. (The PO_4^{3-} ion is precipitated rapidly, probably as hydroxyapatite [10,12].) It is not possible to determine from XRD or NMR data the exact composition of the interlayer anions.

Similar results were obtained using ^{29}Si and ^{27}Al MAS NMR to follow the hydration process of the adiabatically cured samples. In the ^{29}Si MAS NMR spectra (Fig. 9), the peak due to $Q^4(4Al)$ was clearly visible by 24 h of hydration; at later ages, peaks due to C-S-H could be observed. In the later spectra, the peak due to fly ash glass is not readily observed. The intensity of this peak is known to be influenced by the presence of iron in the fly ash glass, and correct quantitative analysis is not possible. In the ^{27}Al MAS NMR (not shown), a sharp peak similar to that due to Al[4] species seen in the aged wasteform becomes predominant by 24 h.

To our knowledge, initial formation of an AFm phase followed by conversion to sodalite has not been previously observed in hydrating cement systems, but because these two phases are principal repositories of anionic species, their involvement in reactions in this complex system is reasonably expected. The AFm phase probably has a +2/+3 ratio (probably mostly Ca/Al) close to 2/1, because these phases show little deviation from this ratio [20]. Sodalite contains Al, Si, Na, and possibly Ca, and various anions. Thus, the conversion of AFm to sodalite cannot involve a simple structural reorganization, but must take place by a through-solution process with substantial com-

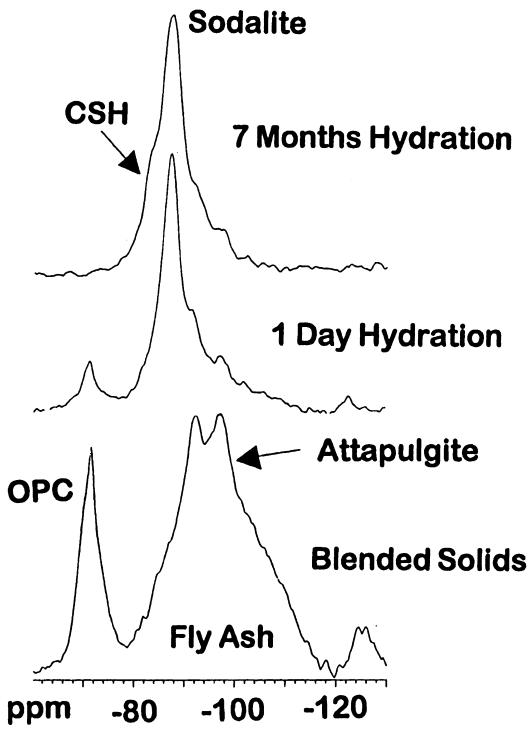

Fig. 9. ^{29}Si MAS NMR spectra showing the evolution of the hydrating wasteform.

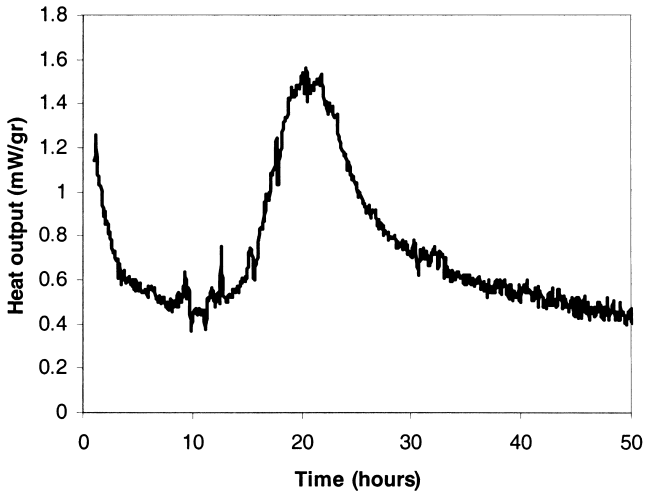

Fig. 10. Conduction calorimetry for the wasteform hydrated isothermally at 45°C.

positional changes and involvement of other species. Formation of sodalite probably occurs from species released by AFm decomposition, and by further reaction of cement and fly ash.

Zeolite Na-P1 begins to appear as a distinct phase by 2 days under adiabatic conditions and at 90°C (Fig. 7(a) and (b)). With isothermal curing at 90°C (Fig. 7(c)), the peaks at 9.3° and 15.8° 2θ (0.95 and 0.55 nm) suggest limited formation of chabazite (possibly sodium substituted). Chabazite is a naturally occurring calcium zeolite of formulae $Ca_2Al_4Si_8O_{24}{\cdot}13H_2O$, and is not easily synthesized [23], although the Cs-substituted analogue forms readily in calcium aluminate cement/silica fume blends hydrated with CsOH [8,9]. However, chabazite does not form under the adiabatic curing conditions likely to be experienced in practice.

The more severe curing regimens also seemed to cause reaction of the attapulgite, with significant quantities of attapulgite only remaining for isothermal curing at 45°C. These results indicate that reaction continues after the initial period of rapid hydration, and that, eventually, high proportions of the fly ash and the clay react (the latter at higher temperatures). If these continuing reactions are exothermic, then the total adiabatic temperature rise may be significantly higher than that predicted from analysis of adiabatic calorimetry data for the first few days of hydration. A higher temperature than predicted could possibly cause unexpected damage to large monoliths made from this wasteform, or to vaults designed with the assumption of the predicted upper temperature limit. If the temperature rose sufficiently high, then problems would also be experienced with pore solution boiling.

3.4. Calorimetry

Isothermal calorimetry of the hydrating samples performed at 45°C (Fig. 10) shows an initial exothermic reaction during the first ~5 h, followed by a period of lower heat output and then a distinct exotherm at approximately 20 h. At this temperature, the majority of the AFm phase forms at about 20 h (Fig. 7(a)). Thus, the hydration of this system is broadly similar to that of OPC, with an initial period of reaction, an induction period, and a period of rapid hydration and formation of the principal product phases. However, there is clearly more heat developed before 10 h.

Adiabatic calorimetry (Fig. 2, line (a)) has been performed by PNL laboratories [3,17] as part of the wasteform development procedure. After an initial period of high heat output (Fig. 2, line (c)), there is reduction of heat output. Their results have been verified here using a home-built adiabatic calorimeter [25]. A distinct exotherm at about 5 h correlates with the formation of the majority of the AFm phase (see Fig. 7(b)). This exotherm is equivalent to the exotherm at 20 h, which occurs during isothermal calorimetry at 45°C. Thus, it appears that the chemistry is largely unchanged by the initial curing conditions.

3.5. Strength development

The compressive strengths of the wasteform samples rose to a maximum recorded value of 8.5 MPa at 14 days and fell significantly thereafter (Fig. 11). Similar results [10,15] were found for samples formulated with a simplified waste solution, as indicated by the components in bold type in Table 1. Samples with a 20% lower liquid/solids ratio continued to gain strength after 14 days [10]. Samples prepared from diluted waste did not lose strength [15]. Variation of solid blend composition was also found to cause significant changes in mineralogy and strength development [37]. Changes in reactivity of the materials, for example, by alteration of the fly ash source, are also likely to cause significant changes. The variability of these results suggests that the strength development depends sensitively

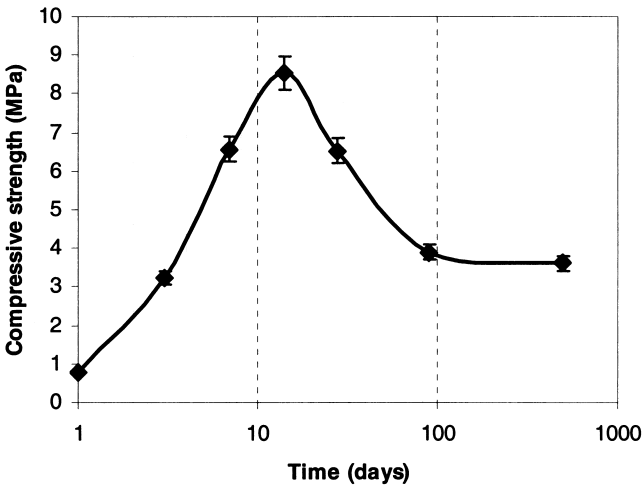

Fig. 11. Strength development of the wasteform cured adiabatically for 3 days and thereafter at 90°C. Coefficients of variation are approximately 5% of the actual compressive strengths.

upon solution concentration, solution binder ratio, and dry blend composition and provenance.

Wasteform samples hydrated isothermally at 45°C and 90°C had 28-day compressive strengths of 5.8 and 6.6 MPa, respectively, compared with 6.5 MPa for the adiabatically cured samples. The similarity of these results suggests that the initial temperature profile is not an important factor in determining the wasteform strength development, despite its effects on early age mineralogy. This observation is consistent with the similar final mineralogy formed under the different curing regimens reported in earlier sections of the paper. The pore solution chemistry also approaches a uniform composition for a range of curing temperatures [10,12], although its rate of change is temperature-dependent.

We do not have an explanation for the loss of strength during the period from 14 to 28 days. Possible causes might include recrystallization of an early-formed C-S-H gel to give the C-S-H, which shows a clear basal spacing. This reaction would reduce the volume of the products and, thus, cause a loss of strength. (Tobermorite formation does not cause strength loss in autoclaved pastes [20] but the high solution/solid ratio in the wasteform is likely to make it more susceptible to strength loss.) Alternatively, it is possible that some of the early-formed C-S-H could be converted into further zeolites, again leading to a reduction in product volume and loss of strength. In the very long term, continued evolution of products might cause further significant changes in the strength, mineralogy, and pore structure of these materials.

Many of the properties of the wasteform will be determined by the physical distribution of the products, and by their chemical compositions. Comprehensive studies incorporating SEM study of the microstructure and extensive SEM and transmission electron microscopy (TEM) microanalysis are required to improve understanding of the composition and distribution of the products, and aid prediction of long-term properties.

4. Conclusions

The reaction of a cementitious binder of high fly ash content (68.3%) with a simulated alkaline waste solution extensively modifies the hydration chemistry of the binder compared to standard OPC hydration. Early formation of AFm phase causes a distinct exotherm after 5 h of adiabatic hydration. The AFm then decomposes, releasing aluminum to form hydrated sodium aluminosilicates (perhaps partially substituted with calcium) that crystallize as sodalite and Na-P1 (gismondine) zeolites. The calcium zeolite chabazite may also form at 90°C, the maximum adiabatic temperature. These materials are not found in ordinary cement systems. The temperature regime over the first few days caused only minor changes in the zeolite mineralogy and was not important in determining the long-term properties of the wasteform. A quasi-crystalline Al-substituted C-S-H gel with a layer spacing of 1.1 nm is also formed. This contains longer silicate chains, and has a higher level of Al substitution and a lower layer spacing relative to C-S-H gel formed by conventional cement hydration at ambient temperature.

In mature wasteforms, further reaction of the fly ash forms more zeolites. This slow ongoing reaction may liberate some additional heat upon prolonged curing, and short-term laboratory experiments may significantly underestimate the long-term adiabatic temperature rise. Clearly, such a temperature rise could cause significant damage to large monoliths of this material, an important practical implication.

There is a major loss of strength after 14 days of hydration; possibly due to recrystallization of the C-S-H gel, or its conversion to zeolites. Continued crystallization could cause significant changes in the pore structures of these materials at later ages. Comprehensive studies incorporating SEM and TEM study of the microstructure and extensive TEM microanalyses would be required to characterize fully the composition and distribution of the products, and to aid prediction of long-term properties.

Acknowledgments

The authors acknowledge the financial support of DOE through the Westinghouse Hanford Co., under Grant No. MJGSVV-097600. Additional support was provided by the NSF Center for Advanced Cement-Based Materials. We thank Mike Cich for assistance with the experimental work, Robert Frost of the Illinois State Geological Survey for performing the XRF analyses, Ben Montez of the School of Chemical Sciences for assistance with the NMR equipment, and Ash Grove Cement (Durkee, OR), Ross Sand and Gravel (Portland, OR), and Engelhard (Inselin, NJ) for the generous supply of raw materials.

References

[1] F.P. Glasser, D.E. Macphee, Immobilisation science of cement systems, Mater. Res. Soc. Bull. 18 (1993) 66–71.
[2] A.R. Brough, A. Katz, T. Bakharev, G.K. Sun, R.J. Kirkpatrick, L.J. Struble, J.F. Young, Microstructural aspects of zeolite formation in alkali activated cement containing high levels of fly ash, in: S. Diamond, S. Mindness, F.P. Glasser, L.W. Roberts, J.P. Skalny, L.D. Wakely (Eds.), Microstructures of Cement Based Systems/Bonding and Interfaces in Cementitious Materials, Mater. Res. Soc. Symp. Proc. 370, Materials Research Society, Pittsburgh, PA, 1995, pp. 199–208.
[3] R.O. Lokken, Heat of hydration of double-shell slurry feed grouts, Report PNL-7860, Pacific Northwest Laboratories, Richland, WA, 1992.
[4] L.L. Ames Jr., The cation sieve properties of clinoptilolite, Am. Min. 45 (1960) 689–700.
[5] S. Kaushal, D.M. Roy, P.H. Licastro, C.A. Langton, Thermal properties of fly ash slag cement waste forms for disposal of SRP salt waste,

in: G.J. McCarthy, F.P. Glasser, D.M. Roy (Eds.), Fly Ash and Coal Conversion By-Products: Characterisation and Disposal II, Mater. Res. Soc. Symp. Proc. 65, Materials Research Society, Pittsburgh, PA, 1986, pp. 311–320.
[6] J.L. LaRosa, S. Kwan, M.W. Grutzeck, Zeolite formation in Class F fly ash blended cements, J. Am. Ceram. Soc. 74 (1992) 1574–1580.
[7] S.L. Hoyle, M.W. Grutzeck, Incorporation of Cs by hydrating calcium aluminosilicates, J. Am. Ceram. Soc. 72 (1989) 1938–1947.
[8] H. Fryda, G. Vetter, R. Ollitraut-Fichet, P. Boch, A. Capmas, Formation of chabazite in mixes of calcium aluminate cement and silica fume used for cesium immobilisation, Adv. Cem. Res. 8 (1996) 29–39.
[9] H. Fryda, R. Boch, K. Scrivener, Formation of zeolite in mixes of calcium aluminate cement and silica fume used for cesium immobilisation, in: K.L. Scrivener, J.F. Young (Eds.), Mechanisms of Chemical Degradation of Cement-Based Systems, E & FN Spon London, 1997, pp. 366–373.
[10] R.A. Olson, P.D. Tennis, D. Bonen, H.M. Jennings, T.O. Mason, B.J. Christensen, A.R. Brough, G.K. Sun, J.F. Young, Early containment of high alkaline solution simulating low-level radioactive waste in blended cement, J. Hazard. Mater. 52 (1997) 223–236.
[11] A. Katz, A.R. Brough, T. Bakharev, R.J. Kirkpatrick, L.J. Struble, J.F. Young, LLW solidification in cement — effect of dilution, in: S. Diamond, S. Mindness, F.P. Glasser, L.W. Roberts, J.P. Skalny, L.D. Wakely (Eds.), Microstructures of Cement Based Systems/ Bonding and Interfaces in Cementitious Materials, Mater. Res. Soc. Symp. Proc. 370, Materials Research Society, Pittsburgh, PA, 1995, pp. 209–216.
[12] S. Sahu, S. Diamond, Pore solution chemistry of simulated low level waste incorporated cement grouts, in: W.M. Murphy, D.A. Knecht (Eds.), Scientific Basis of Nuclear Waste Management XIX, Mater. Res. Soc. Symp. Proc. 412, Materials Research Society, Pittsburgh, PA, 1996, pp. 411–418.
[13] T. Bakharev, A.R. Brough, R.J. Kirkpatrick, L.J. Struble, J.F. Young, Chemical evolution of cementitious materials with high proportion of fly ash and slag, in: K.L. Scrivener, J.F. Young (Eds.), Mechanisms of Chemical Degradation of Cement-Based Systems, E & FN Spon London, 1997, pp. 307–314.
[14] D. Bonen, P.D. Tennis, R.A. Olsen, H.M. Jennings, T.O. Mason, Stabilization of simulated alkaline non-vitrifiable low-level radioactive waste by carbonate bearing AFm and AFt phases, in: K.L. Scrivener, J.F. Young (Eds.), Mechanisms of Chemical Degradation of Cement-Based Systems, E & FN Spon London, 1997, pp. 374–386.
[15] A. Katz, A.R. Brough, R.J. Kirkpatrick, L.J. Struble, J.F. Young, Effect of solution concentration on the properties of cementitious grout wasteform for low level nuclear waste, Nucl. Technol. 129 (2000) 236–245.
[16] R.O. Lokken, J.W. Shage, P.F.C. Martin, Effect of curing temperature on the properties of cementitious wasteforms, in: V.M. Oversby, P.W. Brown (Eds.), Scientific Basis for Nuclear Waste Management XIII, Mater. Res. Soc. Symp. Proc. 176, Materials Research Society, Pittsburgh, PA, 1990, pp. 23–29.
[17] R.O. Lokken, P.F.C Martin, S.E. Palmer, Effect of curing temperature and curing time on double-shell tank waste grouts, Report HGTP-93-0302-01, Pacific Northwest Laboratory, Richland, WA, 1992.
[18] D. Fenzke, D. Freude, T. Frohlich, J. Haase, NMR intensity measurements of half-integer quadrupole nuclei, Chem. Phys. Lett. 111 (1984) 71–175.
[19] S. Diamond, On the glass present in low calcium and high calcium fly ashes, Cem. Concr. Res. 13 (1983) 459–464.
[20] H.F.W. Taylor, Cement Chemistry, Academic Press, New York, 1990.
[21] W.A. Gutteridge, On the dissolution of the interstitial phases in portland cement, Cem. Concr. Res. 9 (1979) 319–324.
[22] L. Struble, The effect of water on maleic acid and salicylic acid extractions, Cem. Concr. Res. 15 (1985) 631–636.
[23] D.W. Breck, Zeolite Molecular Sieves, Wiley-Interscience: New York, 1974.
[24] R.M. Barrer, Hydrothermal Chemistry of Zeolites, Academic Press, London, 1982.
[25] A.R. Brough, unpublished results, 1996.
[26] E. Lippmaa, M. Magi, M. Tarmak, A high resolution ^{29}Si NMR study of the hydration of tricalcium silicate, Cem. Concr. Res. 12 (1982) 597–602.
[27] A.R. Brough, C.M. Dobson, I.G. Richardson, G.W. Groves, In situ solid state NMR studies of Ca_3SiO_5: hydration at room temperature and at elevated temperatures using ^{29}Si enrichment, J. Mater. Sci. 29 (1994) 3926–3940.
[28] I.G. Richardson, A.R. Brough, R. Brydson, G.W. Groves, C.M. Dobson, Location of aluminum in substituted calcium silicate hydrate (C-S-H) gels as determined by ^{29}Si and ^{27}Al NMR and EELS, J. Am. Ceram. Soc. 76 (1993) 2285–2288.
[29] I.G. Richardson, A.R. Brough, G.W. Groves, C.M. Dobson, The characterisation of hardened alkali-activated blast-furnace slag pastes and the nature of the calcium silicate hydrate (C-S-H) phase, Cem. Concr. Res. 24 (1994) 813–829.
[30] G.K. Sun, Unpublished results, 1999.
[31] H.S. Jacobsen, P. Norby, H. Bildsoe, H.J. Jakobsen, 1:1 correlation between ^{27}Al and ^{29}Si chemical shifts and correlation with lattice structures for some aluminosilicate sodalites, Zeolites 9 (1989) 491–495.
[32] R. Tabeta, M. Aida, H. Saito, A high resolution solid state ^{23}Na MAS NMR study of sodium complexes with solvents, small ligand molecules, and ionophores: ^{23}Na chemical shifts as means for identification and characterisation of ion–ion, ion–solvent, and ion–ligand interactions, Bull. Chem. Soc. Jpn. 59 (1986) 1957–1966.
[33] P.B. Kempa, G. Engelhardt, J.Ch. Buhl, J. Felsche, G. Harvey, Ch. Baerlocher, X-ray powder diffraction crystal structure analysis and ^{29}Si and ^{23}Na MAS NMR studies of nitrite sodalite, Zeolites 11 (1991) 558–562.
[34] S. Sahu, S. Diamond, private communication, 1995.
[35] T. Bakharev, private communication, 1995.
[36] A.K. Sarkar, D.M. Roy, A new characterization technique for trimethylsilylated products of old cement pastes, Cem. Concr. Res. 9 (1979) 343–352.
[37] G.-K. Sun, unpublished results, 1995.